

Coherent X-ray Diffractive Imaging; applications and limitations

S. Marchesini, H. N. Chapman, S. P. Hau-Riege, R. A. London, and A. Szöke
Lawrence Livermore National Laboratory, 7000 East Ave., Livermore CA 94550 USA.

H. He, M. R. Howells, H. Padmore, and R. Rosen
Advanced Light Source, Lawrence Berkeley Lab, 1 Cyclotron Rd., Berkeley, CA 94720. USA.

J. C. H. Spence and U. Weierstall
Department of Physics and Astronomy, Arizona State University, Tempe AZ 85287-1504, USA.

The inversion of a diffraction pattern offers aberration-free diffraction-limited 3D images without the resolution and depth-of-field limitations of lens-based tomographic systems, the only limitation being radiation damage. We review our experimental results, discuss the fundamental limits of this technique and future plans.

I. INTRODUCTION

Three ideas, developed over half a century, have now converged to provide a working solution to the non-crystallographic phase problem. In this paper we outline some applications and our development of this solution, which provides a method for lensless, diffraction-limited, aberration-free X-ray imaging of nano-objects in three-dimensions at high resolution. We suggest the acronym CXDI (Coherent X-ray Diffractive Imaging) for this field. We also discuss the fundamental limitations on resolution set by radiation damage, and some new approaches to this problem based on femtosecond diffraction.

The ideas start with Sayre's 1952 observation that Bragg diffraction undersamples diffracted intensity relative to Shannon's theorem [1]. Secondly, the development of iterative algorithms with feedback in the early nineteen-eighties produced a remarkably successful optimization method capable of extracting phase information from adequately sampled intensity data [2]. Finally, the important theoretical insight that these iterations may be viewed as Bregman Projections in Hilbert space has allowed theoreticians to analyze and improve on the basic Fienup algorithm [3]. A parallel development was the real space algorithm for "phase recovery" in crystallography [4] and non-periodic diffraction [5].

Experimental work started for X-rays with the images of lithographed structures reconstructed from their soft-X-ray diffraction patterns by Miao et al. in 1999 [6]. More recently we have seen higher resolution X-ray imaging [7], 3D imaging [7, 8], the introduction of algorithms which do not require a conventional lower-resolution image to provide the boundary (support) of the object [9, 10, 11] and the striking atomic-resolution image of a single nanotube reconstructed from an experimental electron micro-diffraction pattern (an example of the more general CDI method) [12].

The rapid growth of nanoscience (described recently as "the next industrial revolution") has produced an urgent need for techniques capable of revealing the internal structure, in three dimensions, of inorganic nanostructures and large molecules which cannot be crystal-

lized (such as the membrane proteins of vital importance for drug delivery). Scanning probe methods are limited to surface structures, and the electron microscope can provide atomic resolution images of projections of crystalline materials in thicknesses up to about 50nm, or tomography of macromolecular assemblies and inorganics at lower resolution. No technique at present can provide three-dimensional imaging at nanometer resolution of the interior of particles in the micron size range. The development of such a method would have a decisive impact on several fields of science, and would be a timely enabling technology for the Molecular Foundry at Lawrence Berkeley National Laboratory, the Linac Coherent Light Source (LCLS) at Stanford and other nanoscience user facility initiatives. Briefly, we foresee initial applications for CXDI (in the 0.5–4kV X-ray range) in materials science as follows: 1. The visualization of the internal labyrinth structure of the new mesoporous framework structures (eg. glassy foams, now finding uses for molecular sieves and hydrogen storage; 2. Imaging the complex tangles of dislocation lines which are responsible for work-hardening; 3. Imaging the cavities within duplex steels, responsible for their very high uniform extension; 4. 3D imaging defect structures in magnetic multilayers; 5. The tomographic imaging of misfit dislocations at interfaces, free of the thin-film elastic relaxation processes which distort the images obtained by transmission electron microscopy; 6. Imaging of the three-dimensional arrangement of Orowan dislocation loops which, by entanglement with particles, provide the dispersion-hardening of copper alloys; 7. The imaging of precipitates in metal-matrix composite materials; 8. The imaging of electronic device elements for future computing schemes, such as quantum computing. This application is particularly promising, since the ability to prepare the elements lithographically provides the a-priori information needed to solve the phase problem. In life sciences such a technique is needed to determine the bulk (internal) structure of assemblies of macromolecules (molecular machines), protein complexes, and virus particles at a resolution sufficient to recognize known proteins and determine their relationships to each other.

The apparatus we have developed for CXDI is reviewed in section 3 and reconstruction methods are described in section 4. Section 5 summarizes data on the radiation damage limitations to resolution, and the theoretical basis for these limits, while Section 6 describes a method for overcoming those limits by using ultrafast x-ray pulses. We begin by describing a new algorithm for CXDI which avoids the need for *a priori* knowledge of the object support.

II. THE CXDI TECHNIQUE

A CXDI experiment consists of three steps: (a) the sample is illuminated by monochromatic coherent x-rays and a recording is made of a single diffraction pattern (for 2D) or a tilt series (for 3D); (b) the phases of the pattern are recovered from the measured intensities using established phase-retrieval algorithms; (c) the unknown object is then recovered by Fourier inversion. In the Gerchberg-Saxton-Fienup scheme one starts with random phases, which lead to noise when transformed from reciprocal to real space. One then imposes the “finite support” constraint (namely that there must be a blank frame around the specimen), before transforming back to reciprocal space. In reciprocal space the phases so generated are combined with the measured diffraction magnitudes to start the next iteration. After a large number of iterations, in most cases the object emerges from the noise. Our novel improvement is that the estimate for the object support is continually updated by thresholding the intensity of the current object reconstruction [11]. We start from a threshold of the transform of the diffraction pattern and as the iterations progress the support converges to a tight boundary around the object. This, in turn, improves the image reconstruction, which gives a better estimate of the support. An example of the reconstruction of a simulated diffraction pattern produced by a cluster of gold balls is shown in the movie (Fig. 3) together with the support.

The algorithm does not require any “atomicity” constraint provided by the gold balls as demonstrated by the reconstruction of a greyscale image. The algorithm also successfully reconstructs complex objects (those that cause large variations in the phase of the exit wavefield in two dimensions), which hitherto have been experimentally difficult to reconstruct. This opens up the possibility of image reconstruction from microdiffraction patterns, where the illumination is tightly focused on the object.

III. CXDI EXPERIMENTS AT THE ALS

Our experiments in coherent diffraction began with trials using electron [13] and visible-light [14] optics and continued with CXDI at the Advanced Light Source (ALS). The experiments used the “pink” beam at beam-

line 9.0.1 [15] which is fed by a 10-cm-period undulator operating in third harmonic with deflection parameter (K) equal to 1.2 and delivering 588 eV (2.11 nm) photons. Features of the beam line include a 0.5 μm -thick, 750 μm -square Be window to separate the UHV beam line from the low-vacuum sample environment, a monochromator consisting of an off-axis segment of a zone plate and the diffraction experiment itself (Fig. 1).

The x-ray coherence length l_c must be greater than the maximum path difference between any pair of interfering rays, i. e. $l_c > w\theta_{\text{max}}$, where w is the width of the sample and θ_{max} is the maximum diffraction angle. For our geometry and wavelength, $\theta_{\text{max}} = 0.12$ radian and the resolution limit is 8.4 nm. For the 5 μm aperture (effectively the monochromator exit slit) shown in Fig. 1, the resolving power is about 500, the coherence length is then 1 μm and the maximum sample illumination area $8 \times 8 \mu\text{m}^2$. Similarly the (spatial) coherence patch provided by the 5 μm aperture is $10 \times 10 \mu\text{m}^2$. Allowing for an empty (but still coherently illuminated) band around the sample, its allowed size is thus $< 4 \times 4 \mu\text{m}^2$.

We consider now the sampling of the diffraction pattern. The Shannon interval for frequency-space sampling of the *intensity* is $1/(2w) = \Delta/\lambda z$ where z is the sample-to-detector distance and Δ is the detector-plane increment (a 25 μm CCD pixel in our case). For our λ and z values this also leads to a maximum sample width of 4 μm . This is correct (Shannon) sampling of the diffraction-plane *intensity* and twofold *oversampling* in each direction of the diffraction-plane wave amplitude. Note that these limits on the sample size arising from coherence and sampling considerations are not the only ones in effect.

We have carried out three series of experiments, all using test samples made from 50 nm gold balls. The first [9] demonstrated the basic 2D technique with image reconstruction using a support function determined by scanning electron microscopy. The second [9] used a sample intentionally prepared in two separated parts, and reconstruction was achieved using information from the 2D diffraction pattern alone. The third series used a miniature sample-rotation device to collect several tomographic data sets. The picture of the device shown in Fig. 1 (picture width = 7 cm) shows the sample and its rotation spindle and driver. The small black square is the frame of a Si_3N_4 window on which the 3D sample is deposited in a 2.5- μm -wide microfabricated tetrahedron (Fig. 2). Not shown is an angular Vernier scale that was used to measure the rotation angle. Using this apparatus, a set of 150 views with at least a 100 second exposure time per view required about 10 hours. The 3D data generated by the object shown in Fig. 2 are still being analysed.

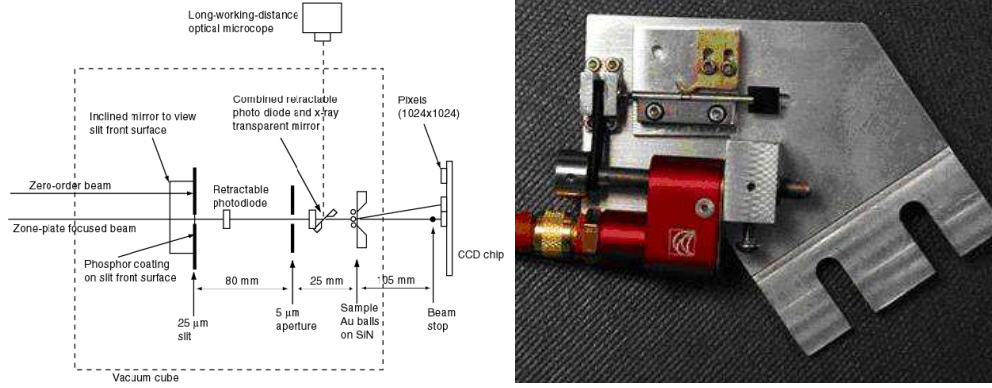


FIG. 1: Experimental chamber layout (left) and rotation device for tomographic recordings (right).

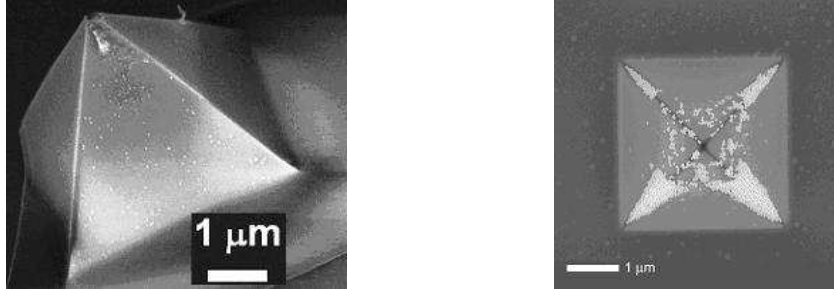


FIG. 2: Three-dimensional test objects fabricated for x-ray diffraction imaging. The left picture shows a SEM perspective image of a silicon nitride pyramid membrane, and the right picture shows a top view of a similar pyramid that has been decorated with 50 nm diameter gold spheres. The silicon nitride is 100 nm thick, and the pyramid is hollow. These objects are ideal for testing since they can be well characterized in the SEM, have extent in all three dimensions, and can be treated as an analogue to a molecule

IV. RECONSTRUCTIONS

Samples were made by placing a droplet of solution containing ‘gold conjugate’ colloidal gold balls on a silicon nitride window (thickness 100 nm) and allowing it to dry. The gold balls formed several single layered (2D) clusters on the SiN membranes, as imaged by a field-emission scanning electron microscope (SEM).

In the first experiment the use of a Si_3N_4 window of the order of 5 microns width ensured that the sample was isolated and of the required size [9]. The structure contained at least one isolated ball generating a ‘reference wave’ which interfered with the signals from other clusters to form a hologram.

The autocorrelation function obtained by Fourier transforming the intensity of the diffraction pattern included an image of every cluster convolved with the single ball, and these images formed a faithful representation of the structure in real space, without iterative processing. Not all the clusters could be imaged this way, since some of the intra-cluster distances were overlapping. The complex transmission function of the Si wedge at the corner of the window generated a complex object that was difficult to reconstruct by phase retrieval. For real objects, we have seen in simulations that using a support of tri-

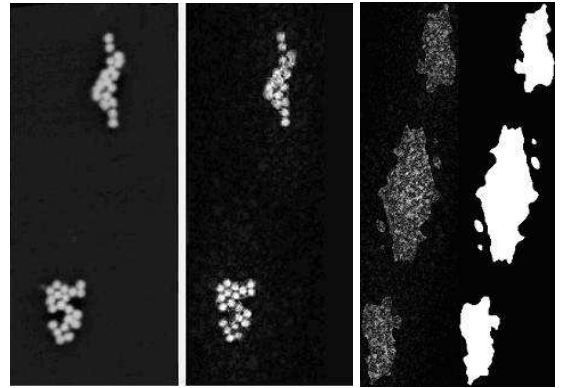


FIG. 3: Comparison of reconstructed soft X-ray image (middle) and SEM images of gold ball clusters (left). Each ball has a diameter of 50nm [H. He, et al. Phys. Rev. B, 67, 174114 (2003)]. Also shown (right) is a movie (1.1 MB) of the reconstruction as it iterates. Each frame of the movie displays the current estimate of the image intensity on the left and the image support on the right [11].

angular shape was sufficient to obtain the image. In the experimental case, we had to use a support obtained from a low resolution image of the object obtained by scanning

electron microscopy (SEM). In the next experiment the object was isolated by means of sweeping the sample particles with an Atomic Force Microscope (AFM). The reconstruction has been obtained using the standard HIO algorithm [2] with missing data due to the beam stop and its supports left unconstrained during the iterations. Rather than rely on a low-resolution secondary imaging method to obtain an estimate of the support, we obtained an estimate of the object support from the support of its autocorrelation. The object support was then adjusted manually as the reconstructed image became clearer [10]. A recently developed algorithm allows both initial support selection and adjustment to be performed automatically [11], extending the technique to objects other than a few separated clusters. This algorithm has been successfully applied on simulated 3D diffraction patterns, and it is being tested on the experimental 3D data recently recorded. We are also investigating the use of the real space algorithm [5] to reconstruct the clusters in Fig. 3 and the 3D data. While this algorithm does require prior information in the form of a low-resolution image, it may be advantageous for the reconstruction from sparse, irregular, incomplete and noisy data.

V. DOSE AND FLUX LIMITATIONS TO PERFORMANCE

In order to assess the promise of CXDI we have carried out calculations intended to determine the fluence (total photons per unit area) and dose (absorbed energy per unit mass) required to make a 3D CXDI image at given resolution. The basis of the calculation was the so-called “dose fractionation” theorem [16, 17]. The theorem states that the radiation dose required to measure the strength of a voxel is the same for a multi-view 3-D experiment (with appropriate reconstruction algorithms) as it is for measurement of the voxel alone, provided that the voxel size and the statistical accuracy are the same in both cases. The results are therefore based on a calculation of diffraction by a single voxel. The conclusions were as follows:

1. The dose (D) and fluence (N) needed to produce P scattered x-rays per voxel into a detector collecting the angle required for resolution d , are given by $N = P/\sigma_s$ and $D = \mu h\nu P/\varepsilon\sigma_s$ where μ is the absorption coefficient, $h\nu$ the photon energy and ε the density.
2. The scattering cross section σ_s of the voxel of size $d \times d \times d$ is given by $\sigma_s = r_e^2 \lambda^2 |\rho|^2 d^4$ (see also [18]) where r_e is the classical electron radius, λ the wavelength and ρ the complex electron density.
3. For resolution d , the dose and fluence scale as d^{-4}
4. For light elements ρ is fairly constant above about 1 keV so the energy dependence of the dose is expected to be quite flat in the range 1- 10 keV.

5. N is dominated by the cross section and scales with the square of photon energy. Moreover, the coherent power of a source of brightness B is $B(\lambda/2)^2$. This implies a fourth-power fluence penalty for increasing the x-ray energy.
6. Therefore one should use the lowest possible x-ray energy consistent with (roughly) $\lambda < d/2$
7. The dose for detecting a 10 nm protein feature against a background of water according to the Rose criterion [19] is shown in Fig. 4. The required imaging dose in the energy range 1-10 keV is roughly 10^9 Gy

Quantitative dose limit: to obtain an estimate of the resolution limit we have plotted a variety of literature values of the dose needed to destroy biological features as a function of feature size (Fig. 1). Also plotted is the required imaging dose. The tentative conclusion from the graph is that the resolution of the crossover, i.e. about 10 nm, should be possible for unlabelled life-science samples although for material-sciences samples the radiation tolerance (and thus the resolution) can be much higher.

Quantitative fluence limit: in our latest experiment at ALS, we collected a full 3D data set at a resolution that we believe to be around 10 nm (although this is not yet supported any reconstructions) in about 10 hours. We project that a beam line *optimized* for this experiment operating on the ALS after its planned performance upgrade would collect diffraction data about 10^4 times faster than now. From 2, above, this should allow the step from 10 nm to around 1 nm resolution for sufficiently radiation-resistant samples.

VI. FEMTOSECOND CXDI, BEYOND THE RADIATION-DAMAGE LIMIT

A way of overcoming the radiation damage limit in x-ray imaging is to use pulses of x-rays that are shorter in duration than the damage process itself. This idea of flash imaging, first suggested by Solem [20, 21], has been proposed to be extended all the way to atomic resolution using femtosecond pulses from an x-ray free-electron laser (XFEL) [22]. The methodology of CXDI could be used in this case to image single molecules [22, 23, 24]. The general concept for imaging non-periodic samples is to inject reproducible samples (macromolecules, complexes, or virus particles) into the XFEL beam, to intersect one particle (and record one diffraction pattern) per pulse.

In the general XFEL experiment the particle orientation in three dimensions will be random and unknown, and the individual diffraction patterns will be noisy (especially at the highest diffracted angles where the highest-resolution orientation information resides). General ideas and methods, developed for “single-particle” reconstructions in cryo-electron microscopy [25, 26], for

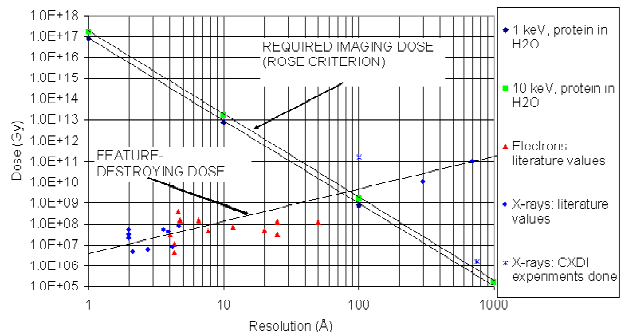
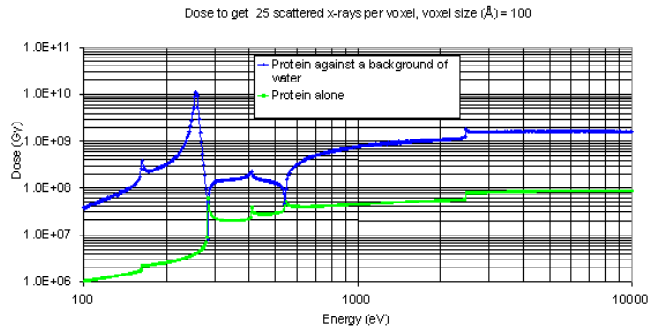


FIG. 4: (left) Plot of dose against x-ray energy. (right) Plot of dose against resolution.

extracting tomographic information from a huge ensemble of randomly oriented noisy images can be applied here. Just as in single-particle EM, the limitations to image resolution are the ability to sort patterns into classes of like-oriented particles, so they can be averaged to improve signal to noise, and the reproducibility of particles. A statistical analysis [27] has shown that signal levels much less than a single count per pixel are adequate to be able to classify diffraction patterns. Even so, due to the exceedingly small scattering cross section of a single macromolecule, pulse fluences of $>10^{12}$ photons per $(100 \text{ nm})^2$ are required to achieve the required signal levels. This corresponds to a dose per particle of $>10^{14}$ Gray. The dose could be reduced substantially if methods could be employed to orient the particle in free space (even if only along a single axis) or if symmetric nanoclusters of particles could be formed.

We have performed calculations to determine, given the required fluence, the longest pulse duration possible to acquire the diffraction pattern before disruption of the electron density of the particle at the atomic scale. The calculation uses a hydrodynamic method treating the electrons and the ions as two separate fluids that interact through the Coulomb force and ionization processes, the assumption being that a large enough macromolecule can be treated as a continuum. Although it does not treat the atomic motions as accurately as the molecular dynamics model [22], the hydrodynamic model is computationally faster and it also enables the inclusion of additional physics effects, in particular the inclusion of the redistribution of free electrons throughout the molecule.

The dominant interactions between the matter and x-ray pulse are K -shell photoionization, (producing damage) and elastic scattering producing the diffraction pattern. Following x-ray absorption in about 2 to 10 fs [28], the K -shell holes decay by emitting Auger electrons with energies in the range of 250 to 500 eV [29]. As the photo and Auger electrons escape they leave behind a molecule with increasing charge and the growing population of low energy secondary electrons becomes trapped and grows still further by collisional ionization (causing the bulk of the damage).

The trapped electrons quickly relax in energy and position to form a neutralizing cloud around the positively charged ions. The particle assumes roughly a two-zone structure, consisting of a neutral core and a positively charged outer shell similar to Debye shielding. On a longer timescale of several 10^3 fs, a macroscopic motion of the whole molecule, called a Coulomb explosion, takes place, leading to an outward radial motion of the ions. The ion motion is greatest within the charged outer layer of the molecule. In the core of the molecule the electron temperature is highest, with the greatest amount of ionization and blurring of the electron density. Preliminary results from the hydrodynamic model indicate that collisional ionization is very rapid and may limit the maximum pulse length to a value smaller than the 10-20 fs inferred by considering only photoionization, Auger ionization and atomic motion. The limits imposed by collisional ionization might be overcome by developing a method to reconstruct atomic positions from partially ionized atoms.

To date it has not been possible to acquire experimental data on the rate of the Coulomb explosion and the effect on electron density of ultrafast high-intensity x-ray pulses. We plan to investigate this at the Tesla Test Facility Phase 2 [30], a soft-x-ray FEL that will be operational in 2004 initially at a wavelength of 20 nm. The first experiments that are planned are to determine the onset of the Coulomb explosion of particles in an aerosol, as a function of pulse fluence, as measured by diffraction from the particles by the x-ray pulses themselves.

VII. CONCLUSIONS

We have discussed advantages and limitations of the CXDI technique, and our progress in implementing the experiments and reconstruction techniques. Preparation of special objects containing an isolated gold ball near an unknown compact object are shown experimentally to allow simple (although low resolution) image reconstruction without iteration based on the autocorrelation function (Fourier transform holography). Such an im-

age may also provide a support function for the retrieval of higher-resolution images using the HIO algorithm. We have developed an algorithm that obtains the support automatically from the autocorrelation function by directly Fourier transforming the recorded diffraction intensity. This eliminates the need for an auxiliary imaging experiment to obtain the support function.

Our last experiment shows that the exposure times for 10 nm resolution are reasonable (about 10 hours) and this resolution is near the dose limit for life-science experiments. Thus we conclude that 3D 10-nm resolution life science experiments on frozen hydrated samples will be possible, and even better resolutions might be achievable with labeling techniques. Calculations indicate that a factor of about 10^4 improvement in imaging speed can be expected using a dedicated CXDI beam line at the upgraded ALS. This is important for applications in material science where the dose limitation is much less severe. Based on the inverse fourth power scaling of the required flux with resolution, this should allow a factor ten improvement in resolution to about 1 nm.

These results have prompted us to develop two parallel projects. One is the development of a program for cryo-CXDI at ALS, and the other aims at femtosecond imaging of single molecules at the LCLS and other 4th generation sources.

The work in CXDI at ALS will be performed in collaboration with groups from NSLS and Stony Brook, who have constructed an instrument designed for collecting 3D data sets [31], and which will be installed at ALS. The instrument incorporates a set of in-vacuum stepper motors for precision positioning the required apertures, beam stop, and diagnostics. It incorporates an air-lock and precision goniometer (developed for electron tomography) for easy introduction and manipulation of the specimen. The specimen holder is designed so as to be able to rotate the specimen over the angular range from -80 to +80 degrees before the specimen supporting grid obscures the beam. A unique feature of the instrument is that a zone plate can be positioned between the specimen and the CCD, thereby a low resolution image of the specimen can be recorded. This feature helps align the specimen, and provides information on its "support".

The key idea to achieving atomic resolution imaging of radiation-sensitive single molecules and particles is that the damage limit may be overcome with the use of very short x-ray pulses to capture the data before damage occurs. Three problems need to be assessed to be able to perform single molecule imaging experiments: fem-

tosecond damage and experiment modeling; image orientation, characterization and reconstruction; and single molecule sample handling.

Fast and accurate hydrodynamic models to describe the interaction of a molecule with femtosecond x-ray pulses needs confirmation from experimental results of short pulse, high-field x-ray-matter interaction experiments planned in the near future. The recorded diffraction patterns must be classified, averaged to increase the signal-to-noise ratio, and oriented for the final 3D reconstruction. Methods developed for single-particle electron microscopy can be applied here. We must also develop methods to inject samples into the beam and, if possible, orient the particles (or at least influence their orientation). Preliminary lower resolution experiments on single particles will provide the answers to the experimental needs to build an experiment at LCLS to perform single-molecule imaging.

We have established the fundamental boundaries of applicability of CXDI to problems in materials and biological sciences. With the rapidly growing importance of nanostructures, and the potential that future developments in this area have for major breakthroughs in the fundamental and applied sciences and in technology, the addition of a new probe that can image thick objects at very high 3d spatial resolution will have a decisive impact on nanoscience and technology. Even more ambitiously, atomic-resolution CXDI at an XFEL, has the potential to provide atomic structure determination of biological systems.

Acknowledgments

We would like to thank Rick Levesque of LLNL for designing and building the rotation stage, and Cindy Larson and Sherry Baker (both LLNL) for SEM imaging. This work was performed under the auspices of the U.S. Department of Energy by the Lawrence Livermore National Laboratory under Contract No. W-7405-ENG-48 and the Director, Office of Energy Research, Office of Basic Energy Sciences, Materials Sciences Division of the U. S. Department of Energy, under Contract No. DE-AC03-76SF00098. SM acknowledges funding from the National Science Foundation. The Center for Biophotonics, an NSF Science and Technology Center, is managed by the University of California, Davis, under Cooperative Agreement No. PHY0120999.

-
- [1] D. Sayre, "Some implications of a theory due to Shannon", *Acta Cryst.* **5**, 843 (1952).
 - [2] J. R. Fienup, "Phase retrieval algorithms: a comparison", *Appl. Opt.* **21**, 2758-2769 (1982).
 - [3] V. Elser, "Phase retrieval by iterative projections", *J. Opt. Soc. Am. A* **20**, 40-55 (2003)
 - [4] A. Szöke, "Holographic microscopy with a complicated reference", *J. Image. Sci. Technol.* **41**, 332-341 (1997).
 - [5] S. P. Hau-Riege, H. Szöke, H. N. Chapman, A. Szöke, "SPEDEN: Reconstructing single particles from their diffraction patterns", *Submitted*, (2003).
 - [6] J. Miao, P. Charalambous, J. Kirz, D. Sayre, "Extend-

- ing the methodology of x-ray crystallography to allow imaging of micrometre-sized non-crystalline specimens”, *Nature* **400**, 342-344 (1999).
- [7] Miao, J., T. Ishikawa, B. Johnson, E. H. Anderson, B. Lai, K. O. Hodgson, “High resolution 3D x-ray diffraction microscopy”, *Phys. Rev. Lett.* **89**, 088303 (2002).
- [8] Williams, G. J., M. A. Pfeifer, I. A. Vartanyants, I. K. Robinson, “Three-Dimensional Imaging of Microstructure in Au Nanocrystals”, *Phys. Rev. Lett.* **90**, 175501 (2003).
- [9] H. He, S. Marchesini, M. R. Howells, U. Weierstall, G. Hembree, J. C. H. Spence, “Experimental lensless soft x-ray imaging using iterative algorithms: phasing diffuse scattering”, *Acta. Cryst.* **A59**, 143-152 (2003).
- [10] H. He, S. Marchesini, M. R. Howells, U. Weierstall, H. Chapman, S. Hau-Riege, A. Noy, J. C. H. Spence, “Inversion of x-ray diffuse scattering to images using prepared objects”, *Phys. Rev. B* **67**, 174114 (2003).
- [11] S. Marchesini, H. He, H. N. Chapman, A. Noy, S. P. Hau-Riege, M. R. Howells, U. Weierstall, J. C. H. Spence, “Imaging without lenses”, arXiv:physics/0306174, (2003).
- [12] Z. M. Zuo, I. Vartanyants, M. Gao, R. Zang, L. A. Nagahara, “Atomic resolution imaging of a carbon nanotube from diffraction intensities”, *Science* **300**, 1419-1421 (2003).
- [13] U. Weierstall, Q. Chen, J. C. H. Spence, M. R. Howells, M. Isaacson, R. R. Panepucci, “Image reconstruction from electron and x-ray diffraction patterns using iterative algorithms: theory and experiment”, *Ultramicroscopy* **90**, 171-195 (2002).
- [14] J. C. H. Spence, U. Weierstall, M. R. Howells, “Phase recovery and lensless imaging by iterative methods in optical, X-ray and electron diffraction”, *Phil. Trans. Roy. Soc. Lond. A* **360**, 875-895 (2002).
- [15] M. R. Howells, P. Charalambous, H. He, S. Marchesini, J. C. H. Spence, “An off-axis zone-plate monochromator for high-power undulator radiation”, in *Design and Microfabrication of Novel X-ray Optics*, D. Mancini, (Ed), Vol. **4783**, SPIE, Bellingham, 2002.
- [16] R. Hegerl, W. Hoppe, “Influence of electron noise on three-dimensional image reconstruction”, *Zeitschrift für Naturforschung* **31a**, 1717-1721 (1976).
- [17] B. F. McEwen, K. H. Downing, R. M. Glaeser, “The relevance of dose-fractionation in tomography of radiation-sensitive specimens”, *Ultramicroscopy* **60**, 357-373 (1995).
- [18] B. L. Henke, J. W. M. DuMond, “Submicroscopic structure determination by long wavelength x-ray diffraction”, *Journal of Applied Physics* **26**, 903-917 (1955).
- [19] A. Rose, “Television pickup tubes and the problem of vision”, in *Advances in Electronics*, Marton, L., (Ed), Vol. **1**, New York, 1948.
- [20] J. C. Solem, G. C. Baldwin, “Microholography of Living Organisms”, *Science* **218**, 229-235 (1982).
- [21] J. C. Solem, G. F. Chapline, “X-Ray Biomicroholography”, *Opt. Eng.* **23**, 193-202 (1984).
- [22] R. Neutze, R. Wouts, D. v. d. Spoel, E. Weckert, J. Hajdu, “Potential for biomolecular imaging with femtosecond x-ray pulses”, *Nature* **406**, 752-757 (2000).
- [23] A. Szöke, “Time resolved holographic diffraction with atomic resolution”, *Chem. Phys. Lett.* **313**, 777-788 (1999).
- [24] J. Miao, K. O. Hodgson, D. Sayre, “An approach to three-dimensional structures of biomolecules”, *Proc. Nat. Acad. Sci.* **98**, 6641-6645 (2001).
- [25] Franck, J., *Three-Dimensional Electron Microscopy of Macromolecular Assemblies*, Academic Press, San Diego, 1996.
- [26] M. v. Heel, B. Gowen, R. Matadeen, E. V. Orlova, R. Finn, T. Pape, D. Cohen, H. Stark, R. Schmidt, M. Schatz, A. Patwardhan, “Single-particle electron cryomicroscopy: towards atomic resolution”, *Quart. Rev. Biophys.* **33**, 269-307 (2000).
- [27] G. Hultdt, A. Szöke, J. Hajdu, “Single Particle Diffraction Imaging: Image Classification”, *Submitted*, (2003).
- [28] E. J. McGuire, “K-Shell Auger Transition Rates and Fluorescence Yields for Elements Be-Ar”, *Phys. Rev.* **185**, 1-6 (1969).
- [29] I. F. Furguson, *Auger Microprobe Analysis*, Adam Hilger, New York, 1989.
- [30] TESLA Test Facility web page, <http://www-hasylab.desy.de/facility/fel/vuv/main.htm> (2003).
- [31] T. Beetz, C. Jacobsen, C. C. Cao, J. Kirz, O. Mentez, C. Sanches-Hanke, D. Sayre, D. Shapiro, “Development of a novel apparatus for experiments in soft x-ray diffraction imaging and diffraction tomography”, *J. de Phys. IV* **104**, 351-359 (2003).